Cyclization of a Cytolytic Amphipathic α-Helical Peptide and Its Diastereomer: Effect on Structure, Interaction with Model Membranes, and Biological Function†

Ziv Oren and Yechiel Shai*

Department of Biological Chemistry, Weizmann Institute of Science, Rehovot, 76100 Israel

Received October 18, 1999; Revised Manuscript Received March 1, 2000

ABSTRACT: The amphipathic α-helical structure is considered to be a prerequisite for the lytic activity of a large group of cytolytic peptides. However, despite numerous studies on the contribution of various parameters to their structure and activity, the importance of linearity has not been examined. In the present study we functionally and structurally characterized a linear amphipathic α-helical peptide (wt peptide), its diastereomer, and cyclic analogues of both. Using analogues with the same sequence of hydrophobic and positively charged amino acids, but with different propensities to form a helical structure, we were able to examine the contribution of linearity to helix formation, bilogical function, and membrane binding and permeation. Importantly, we found that cyclization increases the selectivity between bacteria and human erythrocytes by substantially reducing the hemolytic activity of the cyclic peptides compared with the linear peptides. Moreover, whereas the wt peptide was highly active toward $Gram^+$ bacteria, its cyclic counterpart is active toward both $Gram^+$ and $Gram^-$ bacteria. These findings are correlated with an impaired ability of the cyclic analogues to bind and permeate zwitterionic phospholipid membranes compared with their linear counterparts and an increase in the binding and permeating activity of the cyclic wt peptide toward negatively charged membranes. Furthermore, cyclization abolished the oligomerization of the linear wt peptide in solution and in SDS, suggesting an additional factor that may account for the difference in the spectrum of antibacterial activity between the linear and the cyclic wt peptides. Interestingly, attenuated total reflectance Fourier transform infrared (ATR-FTIR) spectroscopy revealed that, despite cyclization and incorporation of 33% D-amino acids along the peptide backbone, the membrane environment can impose a predominantly helical structure on the peptides, which is required for their bilogical function. Overall, our results indicate that linearity is not a prerequisite for lytic activity of amphipathic α-helical peptides but rather affects the selectivity between $Gram^+$ and $Gram^-$ bacteria and between mammalian cells and bacteria. In addition, the combination of incorporating of D-amino acids into lytic peptides and their cyclization open the way for developing a new group of antimicrobial peptides with improved properties for treating infectious diseases.

The amphipathic α-helical structure is involved in the initial stages leading to the binding of membrane active polypeptides including hormones, signal sequences, and cytolytic peptides. Antimicrobial peptides are a group of natural cytolytic peptides that constitute a major part of the innate immunity of a wide range of organisms including humans (*1*). Antimicrobial peptides provided an important model for the study of critical steps in the insertion, secondary structure formation, and interaction of polypeptides with hydrophobic components of the membrane (*2*−*4*). Many studies have indicated that the peptides require a specific secondary structure and that the common features found in most antimicrobial peptides are that they possess an amphipathic character and a net positive charge. The majority of native antimicrobial peptides are either nonlinear, stabilized by disulfide bridges, or linear (*1*). Nonlinear native antimicrobial peptides adopt mainly or only β-sheet structures with one or more disulfide bonds stabilizing their structures (*1*). Members of this group include α-defensins (*5*), β-defensins (*6*), insect defensins (*7*), protegrins (*8*), tachyplesins (*9*), NK-lysin (*10*), and bactenecin (*11*). Reduction of the disulfide bonds in these peptides severely decreases their antimicrobial activity (*12*−*14*). The second group, linear antimicrobial peptides, vary considerably in chain length, hydrophobicity, and overall distribution of charge. Most of the studies on this group were carried out with amphipathic α-helical peptides (*15*). This group includes the following: (i) cell-selective cytolysins that are toxic only to bacteria, e.g. cecropins, isolated from the cecropia moth (*16*), magainins (*17*), and dermaseptins (*18*) isolated from the skin of frogs; (ii) cytolysins that are not cell-selective, such as the bee venom melittin (*19*) and pardaxin (*20, 21*). Many studies have been conducted on the contribution of structure, amphipathicity, and amino acid composition to the lytic activity of linear amphipathic α-helical peptides (*22*). For example, substitution of D-amino acids or incorporation of proline into them considerably reduced or abolished their antibacterial activity, probably because the α-helical structure was disrupted (*23, 24*). Contrary to these findings, when several D-amino acids were incorporated into native (*25, 26*)

† This research was supported by the Basic Research Foundation administered by the Israel Academy of Sciences and Humanities.

* To whom correspondence should be addressed. Tel: 972-8-9342711. Fax: 972-8-9344112. E-mail: Yechiel.Shai @weizmann.ac.il.

10.1021/bi992408i CCC: $19.00
Published on Web 04/29/2000

and model (*27*) non-cell-selective α-helical cytolytic peptides, the resulting diastereomers lost their cytotoxic effects toward mammalian cells but retained high antibacterial activity.

In agreement with these studies, it has been shown that the replacement of a single D-amino acid at each position along amphipathic model peptides has a limited influence on the α-helical structure measured in 50% TFE/water (*28*). Further NMR studies obtained under similar conditions revealed that replacement of double D-amino acids in the middle of an amphipathic α-helix caused local flexibility in its structure, but the amphipathic helical structure was preserved (*29*). More recently, studies on the role of α-helix formation, as a driving force for membrane binding, were conducted on a diastereomer analogue of melittin (*26*, *30*, *31*). The results indicated that energetic constraints imposed on α-helical formation by incorporating D-amino acids may account for the preferential binding of the peptides to bacteria. These studies suggested that once bound to the negatively charged bacteria, because of electrostatic interactions, the peptide is able to pass an energy barrier and to adopt an amphipathic α-helical structure, which is required for membrane insertion and lysis (*30*, *31*). However, the effect of linearity on the structure and function of cytolytic amphipathic α-helical peptides and their diastereomers has to our knowledge yet not been studied. For this purpose we synthesized and structurally and functionally characterized a linear amphipathic α-helical peptide and its diastereomer (containing both L- and D-amino acids), which could lyse both bacteria and erythrocytes as well as their corresponding cyclic analogues. The peptides were then characterized with regard to their biological activity toward erythrocytes and bacteria, their interaction with model membranes, and their ability to self-assemble in solution and in SDS (a membrane-mimetic environment). The secondary structure of the peptides within zwitterionic (PC) and a net negatively charged (PE/PG) phospholipid membrane was studied using attenuated total reflectance Fourier transform infrared (ATR-FTIR)[1] spectroscopy. Understanding the selective function of the peptides toward bacteria versus erythrocytes, their structure and interaction with model membranes, and their oligomeric state will provide insight into their mode of action and the contribution of helix formation and aggregation to peptide function and selectivity.

MATERIALS AND METHODS

Materials. 4-Methyl benzhydrylamine resin (BHA) and butyloxycarbonyl (Boc) amino acids were purchased from Calibochem-Novabiochem (La Jolla, CA). Other reagents used for peptide synthesis included trifluoroacetic acid (TFA, Sigma), *N*,*N*-diisopropylethylamine (DIEA, Aldrich, distilled over ninhydrin), dicyclohexylcarbodiimide (DCC, Fluka), 1-hydroxybenzotriazole (HOBT, Pierce), and dimethylformamide (peptide synthesis grade, Biolab). Egg phosphatidylcholine (PC) was purchased from Lipid Products (South Nutfield, U.K.). Egg phosphatidylglycerol (PG), phosphatidylethanolamine (PE) (type V, from *Escherichia coli*), and methyl methane thiosulfonate (MMTS) were purchased from Sigma. Cholesterol (extra pure) was supplied by Merck (Darmstadt, Germany) and recrystallized twice from ethanol. Peptide markers for SDS−PAGE were purchased from Fluka. All other reagents were of analytical grade. Buffers were prepared in double glass-distilled water.

Peptide Synthesis and Purification. Peptides were synthesized by a solid-phase method on 4-methyl benzhydrylamine resin (0.05 mequiv) (*32*). The peptides were synthesized with cysteine residues at both their N- and C-termini. The resin-bound peptides were cleaved from the resins by hydrogen fluoride (HF) and, after HF evaporation and washing with dry ether, extracted with 50% acetonitrile/water. HF cleavage of the peptides bound to 4-methyl benzhydrylamine resin resulted in C-terminus amidated peptides. Each crude peptide contained one major peak, as revealed by RP-HPLC, that was 60−80% pure by weight. The peptides were further purified by RP-HPLC on a C_{18} reverse phase Bio-Rad semipreperative column (250 × 10 mm, 300 Å pore size, 5 μm particle size). The column was eluted in 40 min, using a linear gradient of 10−60% acetonitrile in water, both containing 0.05% TFA (v/v), at a flow rate of 1.8 mL/min. Purified peptides were solubilized at low concentration in sodium acetate (pH 7.3), and cyclization was completed after 12 h. The cyclic peptides were further purified by using RP-HPLC and were shown to be homogeneous (∼95%). To obtain linear peptides, the free cysteine containing peptides were treated with methyl methane thiosulfonate (MMTS). The peptides were subjected to amino acid analysis and electrospray mass spectroscopy to confirm their composition and molecular weight.

Preparation of Liposomes. Small unilamellar vesicles (SUV) were prepared by sonication of PC/cholesterol (10:1 w/w) or PE/PG (7:3 w/w) dispersions. Briefly, dry lipid and cholesterol (10:1 w/w) were dissolved in a $CHCl_3$/MeOH mixture (2:1 v/v). The solvents were then evaporated under a stream of nitrogen, and the lipids (at a concentration of 7.2 mg/mL) were subjected to a vacuum for 1 h and then resuspended in the appropriate buffer, by vortexing. The resultant lipid dispersions were then sonicated for 5−15 min in a bath type sonicator (G1125SP1 sonicator, Laboratory Supplies Co., Inc., New York, NY) until clear. The lipid concentrations of the resulting preparations were determined by phosphorus analysis (*33*). Vesicles were visualized using a JEOL JEM 100B electron microscope (Japan Electron Optics Laboratory Co., Tokyo, Japan) as follows. A drop of vesicles was deposited on a carbon-coated grid and negatively stained with uranyl acetate. Examination of the grids demonstrated that the vesicles were unilamellar with an average diameter of 20−50 nm (*34*).

Antibacterial Activity of the Peptides. The antibacterial activity of the peptides was examined in sterile 96-well plates (Nunc F96 microtiter plates) in a final volume of 100 μL as follows. Aliquots (50 μL) of a suspension containing bacteria at a concentration of 10^6 colony-forming units (CFU)/mL in culture medium (LB medium) were added to 50 μL of water containing the peptide in serial 2-fold dilutions in water. Inhibition of growth was determined by measuring the absorbance at 492 nm with a Microplate autoreader El309

[1] Abbreviations used: ATR-FTIR, attenuated total reflectance Fourier transform infrared; BHA, 4-methyl benzhydrylamine resin; Boc, butyloxycarbonyl; CD, circular dichroism; CFU, colony-forming units; HF, hydrogen fluoride; hRBC, human red blood cells; MIC, minimal inhibitory concentration; MMTS, methyl methane thiosulfonate; PBS, phosphate-buffered saline; PC, egg phosphatidylcholine; PE, *Escherichia coli* phosphatidylethanolamine; PG, egg phosphatidylglycerol; RP-HPLC, reverse phase high-performance liquid chromatography; TFA, trifluoroacetic acid; TFE, 2,2,2-trifluoroethanol.

(Bio-tek Instruments), after an incubation of 18−20 h at 37 °C. Antibacterial activities were expressed as the minimal inhibitory concentration (MIC), the concentration at which 100% inhibition of growth was observed after 18−20 h of incubation.

Hemolysis of Human Red Blood Cells (hRBC). The peptides were tested for their hemolytic activities against hRBC. Fresh hRBC with EDTA were rinsed 3 times with PBS (35 mM phosphate buffer/0.15 M NaCl, pH 7.3) by centrifugation for 10 min at 800*g* and resuspended in PBS. Peptides dissolved in PBS were then added to 50 μL of a solution of the stock hRBC in PBS to reach a final volume of 100 μL (final erythrocyte concentration, 5% v/v). The resulting suspension was incubated under agitation for 60 min at 37 °C. The samples were then centrifuged at 800*g* for 10 min. Release of hemoglobin was monitored by measuring the absorbance of the supernatant at 540 nm. Controls for zero hemolysis (blank) and 100% hemolysis consisted of hRBC suspended in PBS and Triton 1%, respectively.

Binding of Peptides to Vesicles. The interaction of the peptides with vesicles consisting of zwitterionic (PC/cholesterol) or negatively charged phospholipids (PE/PG) was characterized by measuring changes in the emission intensity of the peptides' intrinsic tryptophan in SUV titration experiments. Briefly, SUV were added to a fixed amount of peptide (0.5 μM) dissolved in PBS (35 mM phosphate buffer/0.15 M NaCl), pH 7.4, at 24 °C. A 1-cm path length quartz cuvette that contained a final reaction volume of 2 mL was used in all experiments. The fluorescence intensity of the linear peptides was measured as a function of the lipid/peptide molar ratio (4 separate experiments) on a SLM-Aminco, Series 2 spectrofluorometer, with excitation set at 280 nm, using a 4 nm slit, and emission set at 340 nm, using a 4 nm slit. In the case of the cyclic peptides the excitation was set at 280 nm and the emission was set at the emission peak of the peptides in PBS. The binding isotherms were analyzed as a partition equilibrium, using the following formula (*35*, *36*):

$$X_b = K_P C_f$$

Here X_b is defined as the molar ratio of bound peptide (C_b) per total lipid (C_L), K_P corresponds to the partition coefficient, and C_f represents the equilibrium concentration of the free peptide in solution. For practical purposes, it was assumed that the peptides initially were partitioned only over the outer leaflet (60%) of the SUV (*37*). Therefore, the partition equation becomes

$$X_b^* = K_P^* C_f$$

where X_b^* is defined as the molar ratio of bound peptide per 60% of total lipid and K_P^* is the estimated surface partition constant. The curve resulting from plotting X_b^* vs free peptide, C_f, is referred to as the conventional binding isotherm.

Membrane Permeation Induced by the Peptides. Membrane destabilization, which results in the collapse of a diffusion potential, was detected fluorometrically as previously described (*38*−*40*). Briefly, a liposome suspension, prepared in "K^+ buffer" (50 mM K_2SO_4/25 mM HEPES−sulfate, pH 6.8), was added to an isotonic K^+-free buffer (50 mM Na_2SO_4/25 mM of HEPES-sulfate, pH 6.8), and the dye diS-C_2-5 was then added. Subsequent addition of valinomycin created a negative diffusion potential inside the vesicles by a selective afflux of K^+ ions, which resulted in a quenching of the dye's fluorescence. Peptide-induced membrane permeation for all the ions in the solution caused a dissipation of the diffusion potential, as monitored by an increase in fluorescence. Fluorescence was monitored using excitation and emission wavelengths at 620 and 670 nm, respectively. The percentage of fluorescence recovery, F_t, was defined by

$$F_t = [(I_t - I_o)/(I_f - I_o)]100\%$$

where I_t = fluorescence observed after addition of a peptide at time t, I_o = fluorescence after addition of valinomycin, and I_f = total fluorescence prior to the addition of valinomycin.

ATR-FTIR Measurements. Spectra were obtained with a Bruker equinox 55 FTIR spectrometer equipped with a deuterated triglyceride sulfate (DTGS) detector and coupled with an ATR device. For each spectrum, 200 or 300 scans were collected, with resolution of 4 cm^{-1}. During data acquisition, the spectrometer was continuously purged with dry N_2 to eliminate the spectral contribution of atmospheric water. Samples were prepared as previously described (*41*). Briefly, a mixture of PC/cholesterol or PE/PG (1 mg) alone or with peptide (30 μg) was deposited on a ZnSe horizontal ATR prism (80 × 7 mm). The aperture angle of 45° yielded 25 internal reflections. Previous to sample preparations, the trifluoroacetate (CF_3COO^-) counterions which strongly associate to the peptide were replaced with chloride ions through several lyophilizations of the peptides in 0.1 M HCl. This allowed the elimination of the strong C═O stretching absorption band near 1673 cm^{-1} (*42*). Lipid−peptide mixtures were prepared by dissolving them together in a 1:2 $MeOH/CH_2Cl_2$ mixture and drying under a stream of dry nitrogen while moving a Teflon bar back and forth along the ZnSe prism. Polarized spectra were recorded, and the respective pure phospholipids in each polarization were subtracted to yield the difference spectra. The background for each spectrum was a clean ZnSe prism. Hydration of the sample was achieved by introduction of excess of deuterium oxide (^2H_2O) into a chamber placed on top the ZnSe prism in the ATR casting and incubation for 2 h prior to acquisition of spectra. H/D exchange was considered complete due to the complete shift of the amide II band. Any contribution of ^2H_2O vapor to the absorbance spectra near the amide I peak region was eliminated by subtraction of the spectra of pure lipids equilibrated with ^2H_2O under the same conditions.

ATR-FTIR Data Analysis. Prior to curve fitting, a straight baseline passing through the ordinates at 1700 and 1600 cm^{-1} was subtracted. To resolve overlapping bands, the spectra were processed using PEAKFIT (Jandel Scientific, San Rafael, CA) software. Second-derivative spectra accompanied by 13-data-point Savitsky−Golay smoothing were calculated to identify the positions of the components bands in the spectra. These wavenumbers were used as initial parameters for curve fitting with Gaussian component peaks. Position, bandwidths, and amplitudes of the peaks were varied until the following: (i) the resulting bands shifted by

Table 1: Sequences and Designations of the Peptides Investigated

peptide designation	sequence[a,b]
cyclic-K_4L_7W	C K L L L K W L L K L L KC
linear-K_4L_7W	CH_3−S−C K L L L K W L L K L L K C−S−CH_3
cyclic-[D]-$L^{3,4,8,10}$-K_4L_7W	C K L ***L L*** K W L ***L*** K ***L*** L K C
linear-[D]-$L^{3,4,8,10}$-K_4L_7W	CH_3−S−C K L ***L L*** K W L ***L*** K ***L*** L K C−S−CH_3

[a] Italicized and bold amino acids are D-enantiomers. [b] The C-terminal is amidated. [c] CH_3−S is bound to Cys.

Table 2: Minimal Inhibitory Concentration (μM) of the Peptides

	minimal inhibitory concn[a] (μM)				
peptide designation	*E. coli* (D21)	*A. calcoaceticus* (Ac11)	*P. aeruginosa* (ATCC 27853)	*B. subtilis* (ATCC 6051)	*B. megaterium* (Bm11)
cyclic-K_4L_7W	6	4	30	1.5	1
linear-K_4L_7W	150	12.5	100	2	2
cyclic-[D]-$L^{3,4,8,10}$-K_4L_7W	13	5	20	1	1
linear-[D]-$L^{3,4,8,10}$-K_4L_7W	5	2	9	1.5	1
Tetracycline	1.5	1.5	50	6.5	1.2

[a] Results are the mean of 3 independent experiments each performed in duplicates, with standard deviation of 25%.

no more than 2 cm^{-1} from the initial parameters; (ii) all the peaks had reasonable half-widths ($<20-25$ cm^{-1}); (iii) good agreements between the calculated sum of all components and the experimental spectra were achieved ($r^2 > 0.99$). The relative contents of different secondary structure elements were estimated by dividing the areas of individual peaks, assigned to particular secondary structure, by the whole area of the resulting amide I band. The results of four independent experiments were averaged.

Determining the Oligomeric States of the Peptides by SDS−PAGE. The experiments were performed as described in (*43*), except for a change in the sample preparation: HPLC-purified peptide and SDS (1:1 w/w) were dissolved in $CHCl_3$/MeOH (2:1 v/v). The solvents were evaporated under a stream of nitrogen and then lyophilized. Subsequently, the peptides and SDS mixtures were resuspended in buffer composed of 0.065 M Tris-HCl, pH 6.8, and 10% glycerol by sonication. Fixing, staining, and destaining times were 1 min, 1 h, and overnight, respectively, to decrease diffusion effects.

RESULTS

We synthesized linear and cyclic peptides composed of all L-amino acids and their diastereomers. The peptides were short (14 amino acids long) and amphipathic, consisting of positively charged (lysine) and hydrophobic (leucine and tryptophan) amino acids. The linear peptides were prepared by blocking the reduced cysteines with methyl methane thiosulfonate (MMTS), a cysteine-specific reagent. As expected, mass spectroscopy revealed molecular weights of 1805 for the *S*-methyl derivatives and 1711 for the cyclic peptides. Table 1 presents peptide designations and sequences.

Antimicrobial and Hemolytic Activities of the Peptides. The peptides were studied for their potential to inhibit the growth of different species of bacteria. Table 2 gives the MIC for a representative set of test bacteria that includes Gram-negative species: *Escherichia coli*, *Acinetobacter calcoaceticus*, and *Pseudomonas aeruginosa*, and Gram-positive species, *Bacillus subtilis and Bacillus megaterium*. The antibiotic Tetracycline served as a control. The results revealed that cyclization of the L-amino acid peptide and its diastereomer did not affect its activity against Gram-positive bacteria. However, several differences were observed regarding their effect on Gram-negative bacteria. Whereas cyclization of linear-K_4L_7W significantly increased its activity, cyclization of the diastereomer linear-[D]-$L^{3,4,8,10}$-K_4L_7W resulted in a slight decrease in its activity. These results clearly indicate that peptide linearity is not crucial for antibacterial activity, but linearity seems to affect selectivity between Gram-positive and Gram-negative bacteria.

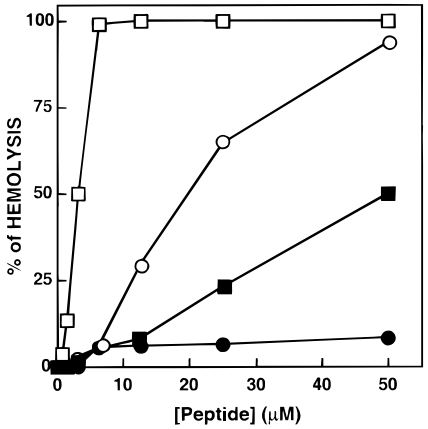

FIGURE 1: Dose−response of the hemolytic activity of the peptides toward hRBC. The assay was performed as described in the Materials and Methods section. Designations are as follows: empty squares, linear-K_4L_7W; filled squares, cyclic-K_4L_7W; empty circles, linear-[D]-$L^{3,4,8,10}$-K_4L_7W; filled circles, cyclic-[D]-$L^{3,4,8,10}$-K_4L_7W.

The peptides were also tested for their hemolytic activity against the highly susceptible human erythrocytes. Figure 1 shows a dose−response curve for the hemolytic activity of the peptides. The results revealed that peptide cyclization substantially decreases the hemolytic activity of both the all L-amino acid peptide and its diastereomer. To ensure that peptide cyclization, rather than the absence of the MMTS blocking groups, is responsible for the decrease in the hemolytic activity of the cyclic peptides, we examined the hemolytic activity of the peptides in the presence of 2 mM DTT. Under these conditions the peptides' disulfide bonds were reduced, as confirmed by mass spectroscopy after RP-

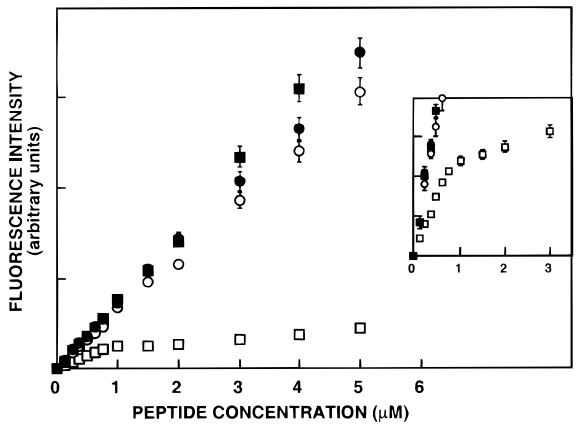

FIGURE 2: Aggregation of the peptides in aqueous solution. The aggregation states of linear-K_4L_7W (empty squares), cyclic-K_4L_7W (filled squares), linear-[D]-$L^{3,4,8,10}$-K_4L_7W (empty circles), and cyclic-[D]-$L^{3,4,8,10}$-K_4L_7W (filled circles) are detected by plotting the concentration dependence fluorescence of the peptides' tryptophan in PBS (35 mM phosphate buffer/0.15 M NaCl, pH 7.4, at 24 °C) in 4 separate experiments. Excitation was set at 280 nm, and emission, at 347 nm. Inset. Magnification of the graph at initial concentrations of the peptides.

HPLC purification. After reduction, the hemolytic activity of the cyclic peptides was the same as their linear analogues, indicating that cyclization rather than blocking the cysteine groups is responsible for their low hemolytic activity. As a control, the hemolytic activity of the bee venom melittin was examined in the presence and absence of DTT. The addition of DTT did not affect the hemolytic activity of melittin (data not shown).

Aggregation of the Peptides in Solution. The aggregational properties of the peptides in aqueous solution (PBS, 35 mM phosphate buffer/0.15 M NaCl, pH 7.4, at 24 °C) were examined using the intrinsic fluorescence probe tryptophan. The dose-dependent fluorescence values of the peptides were recorded at 347 nm (4 separate experiments). Figure 2 depicts the plots of fluorescence versus the concentration of the peptides. The curves obtained for cyclic-K_4L_7W, linear-[D]-$L^{3,4,8,10}$-K_4L_7W, and cyclic-[D]-$L^{3,4,8,10}$-K_4L_7W are linear, suggesting that they do not aggregate. However, the curve obtained for linear-K_4L_7W is strongly bent downward with increasing peptide concentration, suggesting an oligomerization of the peptide. Compared to the other peptides there is a significant quenching in tryptophan fluorescence of linear-K_4L_7W. A possible explanation is that aggregation of the peptide bring to close proximity the two $S-S-CH_3$ disulfide bonds and tryptophans leading to quenching in the tryptophan fluorecensce, since disulfides are known to quench tryptophan fluorescence (*44*, *45*). Another support for the ability of linear-K_4L_7W to oligomerize in solution comes from CD spectroscopy done in PBS at different peptide concentrations ranging from 20 to 60 μM. Linear-K_4L_7W but not its cyclic analogue has a significant α-helical structure (∼30−45%) (data not shown). These results indicate that Linear-K_4L_7W self-associates in aqueous solution to form α-helical structure, as was previously found with other amphipathic α-helical peptides (*46*).

Interaction of the Peptides with Phospholipid Membranes.

Localization of the Environment of Tryptophan. Because of the sensitivity of tryptophan to the polarity of its environment, it has been used for polarity and binding studies (*47*−*50*). To determine the environment of the peptides, we monitored the fluorescence emission spectrum of the tryptophan in PBS at pH 7.2 and in the presence of vesicles composed of either PE/PG (7:3, w/w), a phospholipid composition typical of *E. coli* (*51*), or PC/cholesterol (10:1. w/w), a phospholipid composition used for mimicking the outer leaflet of human erythrocytes (*52*). In these fluorometric studies, SUVs were used to minimize differential light-scattering effects (*53*), and the lipid/peptide molar ratio was maintained high (1000:1) so that the spectral contributions of free peptide would be negligible. The results of this study are summarized in Table 3. In buffer, the tryptophan residue of cyclic-K_4L_7W, linear-[D]-$L^{3,4,8,10}$-K_4L_7W, and cyclic-[D]-$L^{3,4,8,10}$-K_4L_7W exhibited a maximum of fluorescence emission at around 347 ± 2 nm, which reflects a hydrophilic environment for tryptophan (*47*). Linear-K_4L_7W exhibited a slightly lower maximum of fluorescence emission at around 343 ± 2 nm, indicating that tryptophan is less exposed to the aqueous solution. As shown in Figure 2, self-association of the peptide may account for this result. When PE/PG vesicles were added to the aqueous solutions containing the peptides, blue shifts in the emission maxima were observed for all peptides (Table 3). The change in the spectrum of the tryptophan residue reflects its relocation to a more hydrophobic environment (*49*). In the presence of PC/cholesterol vesicles, only linear-K_4L_7W exhibited a blue shift in the emission maxima (toward 339 ± 2 nm). Under our experimental conditions, no blue shift was observed for cyclic-K_4L_7W, linear-[D]-$L^{3,4,8,10}$-K_4L_7W, and cyclic-[D]-$L^{3,4,8,10}$-K_4L_7W, indicating that these peptides do not bind PC/cholesterol vesicles or alternatively, bind them very weakly. Addition of 2 mM DTT to cyclic-K_4L_7W in the presence of PC/cholesterol vesicles resulted in a blue shift in the emission maximum (toward 339 ± 2 nm), as was observed with linear-K_4L_7W. These results further indicate the importance of linearity to the binding of the all L-amino acids peptide to zwitterionic membranes.

Table 3: Tryptophan Emission Maxima of the Peptides in Solution or in the Presence of PE/PG (7:3, w/w) or PC/Cholesterol (10:1, w/w) Vesicles

peptide designation	PBS	PE/PG[a]	PC/cholesterol[a]
cyclic-K_4L_7W	346 ± 1	330 ± 2	346 ± 1
linear-K_4L_7W	343 ± 1	334 ± 2	339 ± 2
cyclic-[D]-$L^{3,4,8,10}$-K_4L_7W	349 ± 1	334 ± 1	349 ± 1
linear-[D]-$L^{3,4,8,10}$-K_4L_7W	349 ± 2	335 ± 1	349 ± 2

[a] A lipid to peptide molar ratio of 1000:1 was used in all cases. Results are the mean of 3 independent experiments.

Binding Studies. The selective cytolytic activity of the peptides may be due to their inability to bind different phospholipid membranes, or alternatively, they may bind but once bound cannot organize themselves into structures that induce membrane lysis. To distinguish between these two possibilities, we conducted a binding study. Briefly, the single tryptophan residue at position 7 of the peptides was used as an intrinsic fluorescence probe to follow the binding of the peptides to model phospholipid membranes. PE/PG (7:3 w/w) and the zwitterionic PC/cholesterol (10:1, w/w) were used in the binding assays. A fixed concentration (0.5 μM) of the linear peptides was titrated using the desired vesicles (PE/PG or PC), and the increase in the fluorescence intensity was followed when binding occurred. Plotting the resulting

increases in the fluorescence intensities of tryptophan as a function of lipid:peptide molar ratios yielded conventional binding curves. No increase in the fluorescence intensity was observed upon titration of both cyclic peptides, cyclic-K_4L_7W and cyclic-[D]-$L^{3,4,8,10}$-K_4L_7W, using PE/PG vesicles. A possible explanation for these results is that conformational changes, that occur upon binding of the peptides to the vesicles place the tryptophan residue in the vicinity of the disulfide bond, which is known to quench the fluorescence of tryptophan (*44*, *45*). However, as depicted in Table 3, both peptides exhibited a blue shift, indicating their binding to PE/PG membranes. Following the decrease in the fluorescence intensity of tryptophan at the emission peak in PBS (which results from the blue shift of the emission maximum) allowed us to follow the binding of the peptides to PE/PG vesicles. Plotting the resulting decrease in the fluorescence intensity of tryptophan (presented as absolute values) as a function of lipid:peptide molar ratios yielded conventional binding curves. The binding curve of linear-K_4L_7W with PE/PG shows that saturation occurred at a lipid:peptide molar ratio of ~10:1 (Figure 3A). A similar result (~8:1) was obtained with cyclic-K_4L_7W (Figure 3B). In the cases of linear-[D]-$L^{3,4,8,10}$-K_4L_7W and cyclic-[D]-$L^{3,4,8,10}$-K_4L_7W, saturation occurred at a higher lipid:peptide molar ratio of ~50:1 (Figure 3A) and ~70:1 (Figure 3B), respectively. Since linear-K_4L_7W aggregates in solution, a binding isotherm was derived only for linear-[D]-$L^{3,4,8,10}$-K_4L_7W, cyclic-K_4L_7W, and cyclic-[D]-$L^{3,4,8,10}$-K_4L_7W by plotting X^*_b (the molar ratio of bound peptide per 60% of the total lipid) versus C_f (the equilibrium concentration of the free peptide in the solution) as shown in the insets of Figure 3A,B. The surface partition coefficient of linear-[D]-$L^{3,4,8,10}$-K_4L_7W was estimated by extrapolating the initial slope of the curves to C_f value of zero and was found to be $1.1(\pm 0.3) \times 10^6$ M^{-1}. The surface partition coefficients of cyclic-K_4L_7W and cyclic-[D]-$L^{3,4,8,10}$-K_4L_7W were found to be $5(\pm 0.4) \times 10^6$ M^{-1} and $0.7(\pm 0.3) \times 10^6$ M^{-1}, respectively. These results reveal that cyclic-K_4L_7W has significantly higher affinity to net negatively charged membranes compared to its diastereomeric analogues, linear-[D]-$L^{3,4,8,10}$-K_4L_7W and cyclic-[D]-$L^{3,4,8,10}$-K_4L_7W.

The shape of the binding isotherm of a peptide can provide information about the organization of the peptide within membranes (*36*). The plot of the binding isotherm of cyclic-K_4L_7W, cyclic-[D]-$L^{3,4,8,10}$-K_4L_7W, and linear-[D]-$L^{3,4,8,10}$-K_4L_7W with PE/PG vesicles is a straight line, which indicates a simple adhesion process, as opposed to cooperativity in binding. These result are in agreement with the inability of cyclic-K_4L_7W, cyclic-[D]-$L^{3,4,8,10}$-K_4L_7W, and linear-[D]-$L^{3,4,8,10}$-K_4L_7W to aggregate in SDS, demonstrating that the dominant form of the peptides is monomer. Similar results were obtained with naturally occurring antibacterial peptides such as dermaseptins (*54*, *55*) and cecropins (*56*, *57*).

Binding studies with PC/cholesterol vesicles revealed no net increase in the tryptophan fluorescence of cyclic-K_4L_7W, linear-[D]-$L^{3,4,8,10}$-K_4L_7W, and cyclic-[D]-$L^{3,4,8,10}$-K_4L_7W nor blue shifts in their emission spectra up to the maximal lipid:peptide molar ratio tested (1000:1). This indicates that the peptides do not bind to PC vesicles or, alternatively, bind very weakly. However, the binding curve of linear-K_4L_7W with PC/cholesterol shows that saturation occurred at a lipid:peptide molar ratio of ~10:1 (Figure 3B), indicating that the peptide has similar affinity to PE/PG and PC/cholesterol membranes.

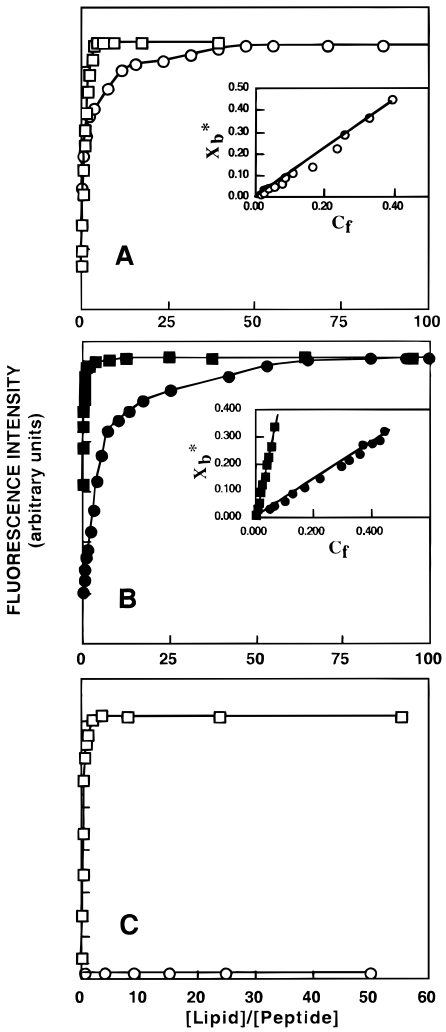

FIGURE 3: Panel A: Increases in the fluorescence of linear-K_4L_7W (empty squares) and linear-[D]-$L^{3,4,8,10}$-K_4L_7W (empty circles) (0.5 μM total concentration) upon titration with PE/PG vesicles, with excitation wavelength set at 280 nm and emission at 340 nm. The experiment was performed at 25 °C in PBS. Inset of panel A: Binding isotherm of linear-[D]-$L^{3,4,8,10}$-K_4L_7W (empty circles) derived from A by plotting X_b* (extent of binding) versus C_f (free peptide). Calculations of X_b* and C_f were performed as described in Material and Methods. Panel B: Changes in the fluorescence of cyclic-K_4L_7W (filled squares) and cyclic-[D]-$L^{3,4,8,10}$-K_4L_7W (filled circles) (0.5 μM total concentration) upon titration with PE/PG vesicles, with excitation wavelength set at 280 nm and emission at 346 nm, in the case of cyclic-K_4L_7W, or 349 nm, in the case of cyclic-[D]-$L^{3,4,8,10}$-K_4L_7W. Inset of panel B: Binding isotherm of cyclic-K_4L_7W (filled squares) and cyclic-[D]-$L^{3,4,8,10}$-K_4L_7W (filled circles). Panel C: Increase in the fluorescence of linear-K_4L_7W (empty squares) and linear-[D]-$L^{3,4,8,10}$-K_4L_7W (empty circles) (0.5 μM total concentration) upon titration with PC/cholesterol vesicles, with excitation wavelength set at 280 nm and emission at 340 nm.

Membrane Permeation Induced by the Peptides. The peptides were mixed at various concentrations with either negatively charged PE/PG vesicles (7:3 w/w) or zwitterionic PC/cholesterol vesicles (10:1, w/w) that had been pretreated with the fluorescent dye, diS-C_2-5, and valinomycin. The kinetics of the fluorescence recovery was monitored with time, and the maximum level reached as a function of peptide concentration was determined. Cyclic-K_4L_7W, linear-[D]-$L^{3,4,8,10}$-K_4L_7W, and cyclic-[D]-$L^{3,4,8,10}$-K_4L_7W were found to

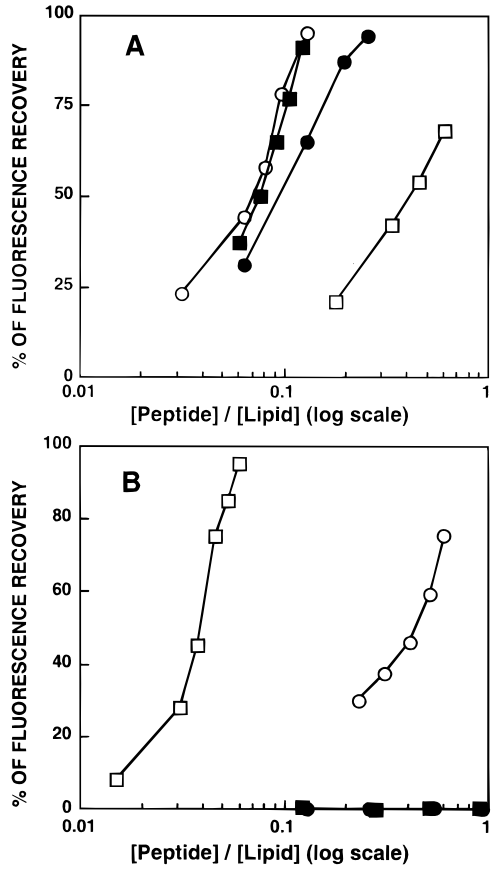

FIGURE 4: Maximal dissipation of the diffusion potential in vesicles induced by the peptides. The peptides were added to isotonic K^+-free buffer containing SUV composed of PE/PG (panel A) or PC/cholesterol (panel B), preequilibrated with the fluorescent dye 3,3′-diethylthiodicarbocyanine iodide and valinomycin. Fluorescence recovery was measured 5−15 min after the peptides were mixed with the vesicles. Cyclic-K_4L_7W and cyclic-[D]-$L^{3,4,8,10}$-K_4L_7W did not exhibit permeating activity on PC/cholesterol up to the maximal peptide:lipid molar ratio tested (1:1). Designations are as follows: empty squares, linear-K_4L_7W; filled squares, cyclic-K_4L_7W; empty circles, linear-[D]-$L^{3,4,8,10}$-K_4L_7W; filled circles, cyclic-[D]-$L^{3,4,8,10}$-K_4L_7W.

permeate PE/PG vesicles with similar and significantly higher potency than linear-K_4L_7W (Figure 4A). These results are correlated with the results obtained in the antibacterial assay with *E. coli*. To rule out the possibility that oligomerization resulting from nonspecific disulfide bonds formation, is responsible for the lower ability of linear-K_4L_7W to permeate PE/PG vesicles, the assay was repeated with linear-K_4L_7W and cyclic-K_4L_7W in the presence of 2 mM DTT. Under these reducing conditions both peptides had the same activity.

In contrast to its low permeating activity with negatively charged membranes, linear-K_4L_7W exhibited high potency with zwitterionic PC/cholesterol membranes, followed by linear-[D]-$L^{3,4,8,10}$-K_4L_7W with significantly lower activity (Figure 4B). The two cyclic peptides, cyclic-K_4L_7W and cyclic-[D]-$L^{3,4,8,10}$-K_4L_7W, did not exhibit permeating activity up to the maximal peptide:lipid molar ratio tested (1:1). To confirm that peptides' cyclization, rather than the absence of the MMTS blocking groups, is responsible for the differences in the membrane permeating activities of the linear peptides and their cyclic analogues, the assay was repeated with the cyclic peptides in the presence of 2 mM DTT. The results revealed that the activity of the cyclic peptides was converted to the higher activity of the linear peptides, indicating that cyclization, rather than the absence of the MMTS blocking groups, is responsible for the reduced activity of the peptides toward PC/cholesterol membranes. With the exception of linear-[D]-$L^{3,4,8,10}$-K_4L_7W the results of this study are in good agreement with the results of the binding study of the peptides to zwitterionic membranes. A possible explanation for the inability to detect the binding of linear-[D]-$L^{3,4,8,10}$-K_4L_7W to PC/cholesterol while observing its permeating activity is the substantially higher concentration of peptide employed in the permeating study (5−10 μM) compared to the binding study (0.5 μM).

Secondary Structure of the Diastereomers in PE/PG and PC/Cholesterol Phospholipid Membranes As Determined by FTIR Spectroscopy. FTIR spectroscopy was used to determine the secondary structure of the peptides within phospholipid membranes. Helical and unordered structures can contribute to the amide I vibration at almost identical wavenumbers, and it is difficult to determine precise proportion of helix and random coil from the IR spectra. However, the exchange of hydrogen with deuterium makes it possible, sometimes, to differentiate α-helical components from random structure, since the absorption of the random structure shifts to a higher extent than the α-helical component after deuteration. Therefore, we examined the IR spectra of the peptides after complete deuteration. The spectra of the amide I region of linear-K_4L_7W and cyclic-K_4L_7W bound to PE/PG (7:3 w/w) multibilayers are shown in Figure 5A,C, respectively, and those for linear-[D]-$L^{3,4,8,10}$-K_4L_7W and cyclic-[D]-$L^{3,4,8,10}$-K_4L_7W are shown in Figure 6A,C, respectively. In addition, spectra of the amide I region were also taken in a zwitterionic 10:1 PC/cholesterol (w/w) multibilayer. Cyclic-K_4L_7W and cyclic-[D]-$L^{3,4,8,10}$-K_4L_7W do not bind or permeate PC/cholesterol and therefore were not examined. The spectrum of linear-K_4L_7W is shown in Figure 7A, and that of linear-[D]-$L^{3,4,8,10}$-K_4L_7W is shown in Figure 7B. Second-derivative accompanied by 13-data-point Savitsky−Golay smoothing were calculated to identify the positions of the component bands in the spectra and are given in the corresponding panels of B and D in Figures 5−7. These wavenumbers were used as initial parameters for curve fitting with Gaussian component peaks. The assignments, wavenumbers (ν), and relative areas of the component peaks are summarized in Table 4.

Assignment of the different secondary structures to the various amide I regions was calculated according to the values taken from Jackson and Mantsch (*58*). The amide I region between 1625 and 1640 cm^{-1} is characteristic of a β-sheet structure, and the region between 1648 and 1655 cm^{-1} is characteristic of an α-helical structure. The assignment of the amide I region between 1670 and 1680 cm^{-1} remains uncertain. Previous studies have correlated this region with β-turns (*59*), possibly sterically constrained non-hydrogen-bonded amide C═O groups within turns (*60*), or the high-frequency β-sheet component (*61*), which arises as a result of transition dipole coupling (*62*).

The linear wt peptide, linear-K_4L_7W, has a tendency to form α-helical structure, as deduced from the major amide I band centered at 1651 cm^{-1} in both the PE/PG and PC/cholesterol membrane and the pronounced α-helical structure observed in 40% 2,2,2-trifluoroethanol (TFE)/water in a circular dichroism study (data not shown). Incorporation of D-amino acids resulted in amide I band shift and increased

Table 4: Assignment, Wavenumbers (ν), and Relative Areas of the Component Peaks Determined from the Deconvolution of the Amide I Bands of the Peptides Incorporated into PE/PG (7:3 w/w) and PC/Cholesterol (10:1 w/w) Multibilayers[a]

	linear-K_4L_7W		cyclic-K_4L_7W		linear-[D]-$L^{3,4,8,10}$-K_4L_7W		cyclic-[D]-$L^{3,4,8,10}$-K_4L_7W	
assgnt	ν (cm^{-1})	area (%)	ν (cm^{-1})	area (%)	ν (cm^{-1})	area (%)	ν (cm^{-1})	area (%)
				PE/PG				
α-helix	1651 ± 1	80 ± 5	1649 ± 1	92 ± 4	1648 ± 1	74 ± 4		
dynamic helix							1657 ± 1	72 ± 2
β-sheet	1628 ± 2	15 ± 2			1625 ± 2	4 ± 1	1636 ± 2	21 ± 3
β-sheet/turn	1679 ± 1	5 ± 3	1680 ± 2	8 ± 4	1673 ± 1	22 ± 3	1681 ± 1	7 ± 2
				PC/Cholesterol				
α-helix	1651 ± 1	80 ± 5			1653 ± 2	60 ± 5		
random coil					1643 ± 2	30 ± 5		
dynamic helix								
β-sheet	1633 ± 2	15 ± 3						
β-sheet/turn	1678 ± 1	5 ± 3			1675 ± 2	10 ± 2		

[a] A 1:80 peptide:lipid molar ratio was used. All values are given as mean ± standard deviation. The results are the mean of 4 independent experiments.

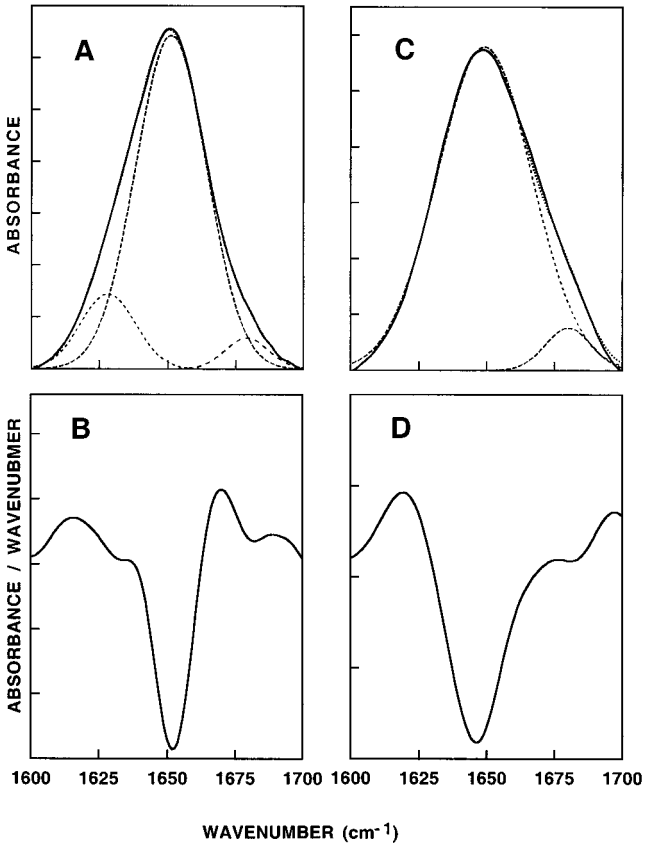

FIGURE 5: FTIR spectra deconvolution of the fully deuterated amide I band (1600−1700 cm^{-}) of linear-K_4L_7W (panel A) and cyclic-K_4L_7W (panel C) in PE/PG (7:3, w/w) multibilayers. The second derivatives, calculated to identify the positions of the components bands in the spectra, are shown in panel B for linear-K_4L_7W and in panel D for cyclic-K_4L_7W. The component peaks are the result of curve-fitting using a Gaussian line shape. The amide I frequencies characteristic of the various secondary-structure elements were taken from ref *58*. The sums of the fitted components superimpose on the experimental amide I region spectra. In panels A and C, the continuous lines represent the experimental FTIR spectra after Savitzky−Golay smoothing; the broken lines represent the fitted components. A 80:1 lipid/peptide molar ratio was used.

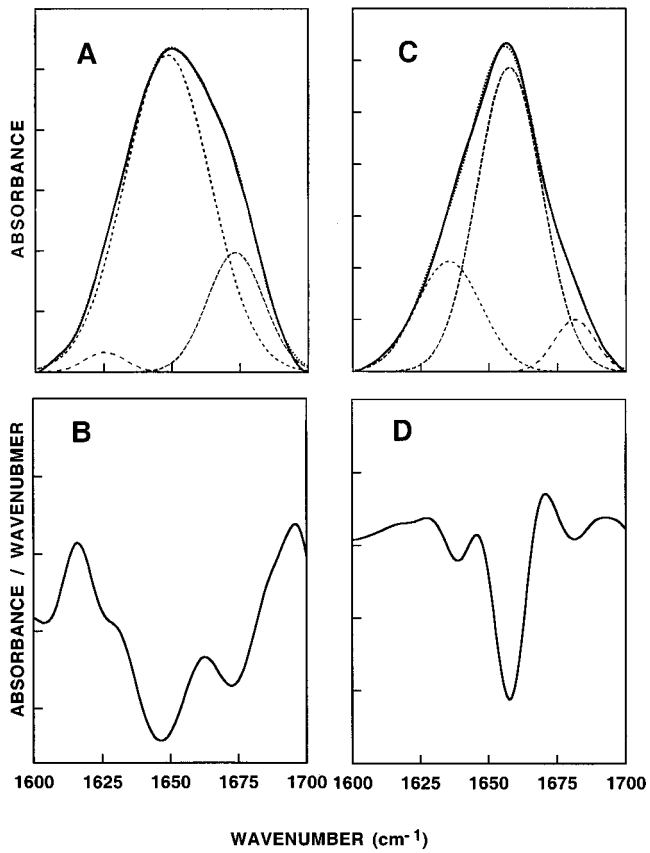

FIGURE 6: FTIR spectra deconvolution of the fully deuterated amide I band (1600−1700 cm^{-1}) of linear-[D]-$L^{3,4,8,10}$-K_4L_7W (panel A) and cyclic-[D]-$L^{3,4,8,10}$-K_4L_7W (panel C) in PE/PG (7:3, w/w) multibilayers. Second derivatives plots of linear-[D]-$L^{3,4,8,10}$-K_4L_7W and cyclic-[D]-$L^{3,4,8,10}$-K_4L_7W are shown in panels B and D, respectively. Details are as depicted in the legend to Figure 5. A 80:1 lipid/peptide molar ratio was used.

peak width, suggesting a higher flexibility of the α-helical structure of linear-[D]-$L^{3,4,8,10}$-K_4L_7W. To directly examine this possibility we conducted an amide hydrogen/deuterium (H/D) exchange experiments. The more stable the hydrogen bonds of the helical structure, the longer it takes to replace the hydrogen atoms with deuterium. When linear-K_4L_7W was exposed to ^2H_2O, the amide II band completely shifted to lower frequency after ∼15 min, while only ∼5 min was required to shift the amide II band of linear-[D]-$L^{3,4,8,10}$-K_4L_7W. This result further indicates that the α-helical structure of linear-[D]-$L^{3,4,8,10}$-K_4L_7W is more flexible than linear-K_4L_7W. Similar results were previously observed in studies that replaced one or two D-amino acids in longer amphipathic model peptides (*28, 29*), and more recently in a NMR study of a diastereomer of melittin (*31*). However,

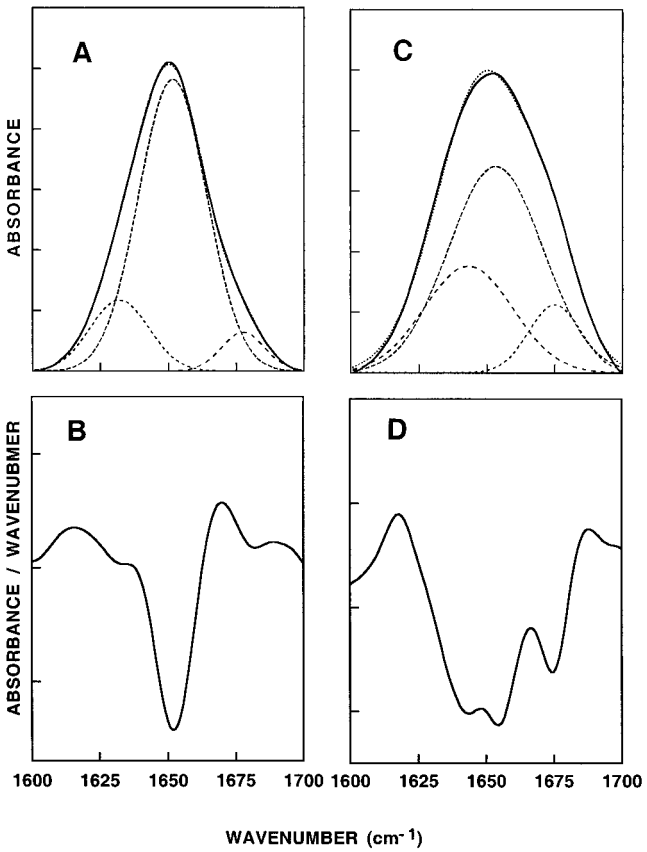

FIGURE 7: FTIR spectra deconvolution of the fully deuterated amide I band (1600−1700 cm^{-1}) of linear-K_4L_7W (panel A) and linear-[D]-$L^{3,4,8,10}$-K_4L_7W (panel C) in PC/cholesterol (10:1 w/w) multibilayers. Second derivatives plots of linear-K_4L_7W and linear-[D]-$L^{3,4,8,10}$-K_4L_7W are shown in panels B and D, respectively. Details are as depicted in the legend to Figure 5. A 80:1 lipid/peptide molar ratio was used.

the major amide I peak center of linear-[D]-$L^{3,4,8,10}$-K_4L_7W is still located in the α-helical range (*58*). Note that in contrast to linear-K_4L_7W, significant differences were observed in the amide I spectrum of linear-[D]-$L^{3,4,8,10}$-K_4L_7W when bound to PE/PG and PC membranes. The major amide I band at 1648 cm^{-1} found with PE/PG membranes was split into a major (∼60%) α-helical band at 1653 cm^{-1} and a smaller (∼30%) random coil band at 1643 cm^{-1}.

Interestingly, cyclization had only slight effect on the α-helical structure of linear-K_4L_7W in PE/PG membrane, as revealed by the slight decrease in the major amide I band located at 1649 cm^{-1}. In contrast, the major amide I bands of cyclic-[D]-$L^{3,4,8,10}$-K_4L_7W are centered at ∼1657 cm^{-1} in PE/PG membranes. This frequency is significantly higher than the frequency of the major amide I band of linear-K_4L_7W centered at 1651 cm^{-1}. We therefore assigned the major band of cyclic-[D]-$L^{3,4,8,10}$-K_4L_7W to dynamic, more flexible helix, as was previously suggested in a study that examined structural changes in phospholipase A_2 (*63*). The results of this study revealed that, upon membrane binding, the α-helical peak of the protein at ∼1650 cm^{-1} was shifted to ∼1658 cm^{-1}, concomitant with extensive H/D exchange rate, indicating destabilization of the α-helical structure. The assignment of the component at ∼1657 cm^{-1} to dynamic helix is further supported by studies that examined distorted α-helical structures (α_{II} helices) in bacteriorhodopsin and other proteins (*64*, *65*). These studies demonstrated that

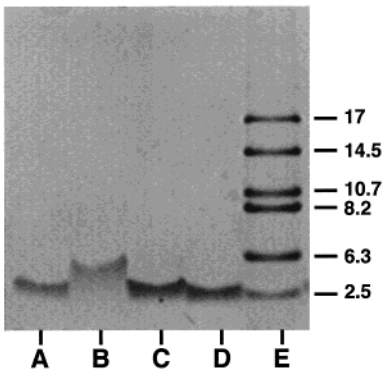

FIGURE 8: Determining the aggregation states of the peptides by Tricine SDS−PAGE. The molecular weight of the linear peptides, linear-[D]-$L^{3,4,8,10}$-K_4L_7W (lane A) and linear-K_4L_7W (lane B), is 1805 Da, and the molecular weight of the cyclic peptides, cyclic-[D]-$L^{3,4,8,10}$-K_4L_7W (lane C), and cyclic-K_4L_7W (lane D), is 1711 Da. Lane E shows the molecular weight markers.

distorted α-helical structures are characterized by increased amide I frequencies.

The β-sheet structure observed in all the peptides may arise from either intermolecular interaction due to peptide aggregation or, most likely in the case of the cyclic peptide, from intramolecular interaction. Another possibility is that this band arises from extended conformation stabilized by interaction of amino acids with membrane components such as the lipid phosphate group and the hydrophobic core of the membrane.

Oligomerization of the Peptides in SDS−PAGE. The state of aggregation of several membrane proteins was determined in SDS, a membrane-mimetic environment (*66*, *67*). Here, SDS−PAGE revealed that the dominant form of linear-[D]-$L^{3,4,8,10}$-K_4L_7W, cyclic-[D]-$L^{3,4,8,10}$-K_4L_7W, and cyclic-K_4L_7W is a monomer, whereas linear-K_4L_7W forms an oligomer, presumably a dimer (Figure 8). As a control, a sample containing cyclic-K_4L_7W was treated with 2 mM DTT, followed by HPLC purification. After reduction, the dominant form of cyclic-K_4L_7W was oligomer, as was observed with linear-[D]-$L^{3,4,8,10}$-K_4L_7W (data not shown).

DISCUSSION

Although many studies on the contribution of structure, amphipathicity, and positive charges to the activity of linear amphipathic cytolytic peptides have been carried out, the importance of linearity has not been examined before. All the peptides studied here have the same sequence of hydrophobic and positively charged amino acids and therefore allowed us to focus the study on elucidating the effect of linearity on function and selectivity.

The results presented here will be discussed considering three interesting findings: (i) Cyclization significantly increased the selectivity between bacteria and mammalian cells, i.e., reducing the hemolytic activity of both linear peptides (Figure 1) while increasing the activity of the wt peptide toward Gram-negative bacteria (Table 2). (ii) Despite cyclization and incorporation of 33% D-amino acids along the peptide backbone, the cyclic peptides can still adopt a predominantly helical structure when bound to the membrane. (iii) Cyclization affects the oligomeric state of the linear wt peptide in solution and a membrane-mimetic environment.

The data reveal a direct correlation between biological function, binding, and permeating model membranes in this group of peptides. Only the most hemolytic peptide, linear-K_4L_7W, binds strongly and permeates most efficiently PC/cholesterol membranes, used to mimic the major components of the outer leaflet of erythrocytes. It should be noted that in addition to PC and cholesterol (up to 40%), the outer leaflet of erythrocytes is composed of sphingomyelin, proteins, and small amount of glycolipids such as globoside (*52*). However, model membranes composed of PC/cholesterol are widely used to examine the interaction of antimicrobial peptides with zwitterionic membrane, typical of normal mammalian plasma membrane, as opposed to the net negatively charged membranes of bacteria (*4, 68*). All the peptides bind and permeate PE/PG vesicles (used to mimic the phospholipid composition of *E. coli* (*51*)) (Figures 3 and 4) with linear-K_4L_7W having the lowest activity, in agreement with its weak activity toward *E. coli*. These results differ from those observed with native amphipathic α-helical antimicrobial peptides. Specifically, magainin, dermaseptins, cecropins, and the human LL-37 are not, or are only weakly, hemolytic. However, they still bind and permeate zwitterionic membranes, similarly (*69, 70*) or with a 10-fold higher concentration compared with that needed for negatively charged membranes (*54, 57, 71*).

One of the models for the conformational changes following the insertion process of amphipathic α-helical peptides into membranes, include interfacial binding in an unfolded state, secondary structure formation, and insertion of a secondary structure units into the lipid bilayers (*72*). According to this model the nonpolar amino acid residues of the amphipathic α-helix will be able to enter the bilayer interior only if they can adopt configuration that satisfies their hydrogen bonds (*72*). In a monomeric form, α-helix is the most likely configuration that will satisfy this requirement. Thus, this model emphasizes the importance of helix formation for membrane binding and is supported by a study that examined the conformational changes of melittin upon interaction with phospholipids (*73*). The results showed that melittin adsorbed on the lipid layer surface contains less α-helix than its counterpart inserted into the membrane. As the melittin depth of penetration is increased, more ordered structure (α-helix) appears. Further support for this model was obtained in a more recent study that examined the binding of the antimicrobial peptide magainin to zwitterionic POPC (1-palmitoyl-2-oleoyl-*sn*-glycero-3-phosphocholine) membranes, using isothermal titration calorimetry combined with CD spectroscopy (*4*). The results of thermodynamic calculations indicated that a membrane-facilitated random coil-to-α-helix transition was the main driving force for magainin binding to lipid membrane.

The results of the present ATR-FTIR studies revealed that linear-K_4L_7W has a high tendency to form an α-helical structure in both zwitterionic and negatively charged membranes. Incorporation of D-amino acids and cyclization increased the flexibility of the α-helical structure, when bound to negatively charged PE/PG membranes, as deduced from the amide I band shift and the peak width (Figure 5 panels C and D and Figure 6 panels A−D). However, the amide I peak center of cyclic-K_4L_7W, linear-[D]-$L^{3,4,8,10}$-K_4L_7W, and cyclic-[D]-$L^{3,4,8,10}$-K_4L_7W is still located in the helical structure range (*58*). These results indicate that a helical structure will remain without appreciable disturbance, despite the presence of D-amino acids and cyclization in a segment with high tendency to form a helical conformation. Our results further indicate that conformational constraints imposed on helix formation by incorporating D-amino acids and cyclization may account for the preferential binding of the peptides to negatively charged membranes. Evidence supporting this hypothesis was presented in several studies that compared the interaction of native melittin and its diastereomer ([D]-$V^{5,8}$,I^{17},K^{21}-melittin, D-amino acids at positions $V^{5,8}$,I^{17},K^{21}) with zwitterionic and negatively charged phospholipids (*26, 30, 31*). [D]-$V^{5,8}$,I^{17},K^{21}-melittin binds strongly and destabilizes only negatively charged phospholipid vesicles, in contrast to native melittin, which binds also strongly zwitterionic phospholipids. The free energies of transfer of melittin and [D]-$V^{5,8}$,I^{17},K^{21}-melittin from the aqueous phase to the membrane of zwitterionic palmitoyloleoylphosphatidylcholine (POPC) were measured using equilibrium dialysis (*30*). The results revealed that more energy has to be invested in the folding of [D]-$V^{5,8}$,I^{17},K^{21}-melittin compared with native melittin (*30*). Therefore, the peptide may be released from the zwitterionic membranes before it forms an α-helical structure.

Electrostatic interactions between the cationic peptides and acidic lipids have been suggested to be mainly responsible for the binding and selective action of antimicrobial peptides on negatively charged bacterial membranes (*74*). In contrast, at the outer leaflet of human erythrocytes (representative of normal mammalian cells), which is predominantly composed of zwitterionic (PC) and sphingomyelin phospholipids (*52*), the peptides encounter electrostatic repulsion. Indeed, studies with several antimicrobial peptides (*25*−*27*, *30*, *54*−*57*, *71*, *75*−*80*) revealed low affinity to zwitterionic phospholipids compared with acidic phospholipids.

Since all the peptides examined in this study carry the same net positive charge, they encounter the same attractive/repulsive electrostatic interaction at the headgroup region. Thus, their distinct binding and permeating properties can be generally explained by their different propensities to form a helical structure. To form a helical structure the cyclic and the diastereomer peptides probably have to cross an energy barrier, resulting from destabilization of the helical structure by cyclization and incorporation of D-amino acids. Our results indicate that the electrostatic attraction between the positively charged cyclic and diastereomeric peptides and the negatively charged membranes may allow the peptides to cross the energy barrier and form a stable helical structure that allows them to penetrate into the membrane as revealed in the binding, tryptophan blue shift, and ATR-FTIR studies.

The second factor that accounts for the differences between the linear and the cyclic all L-amino acids peptides is self-association in solution and possibly in the membrane-bound state. In addition to the effect of cyclization on structure, it most likely affects the ability of the peptide to aggregate. This effect is more significant with the all L-amino acids peptide than with its diastereomer. This property was demonstrated both in aqueous solution (Figure 2) and in a membrane-mimetic environment (SDS−PAGE experiment, Figure 8), as has been done with several other membrane proteins (*66, 67*). The results revealed that in both aqueous solution and the membrane-mimetic environment linear-

K_4L_7W is aggregated, whereas the dominant form of cyclic-K_4L_7W is a monomer.

Preventing the formation of aggregates by cyclization significantly increased the activity of the wild-type peptide linear-K_4L_7W (up to 25-fold) with respect to Gram-negative bacteria while preserving its activity toward Gram-positive bacteria (Table 2). A possible explanation for these results is as follows: With Gram-negative bacteria, the site most likely to be the target of membrane-permeating antibacterial peptides is the inner membrane, which typically contains the electron transport chain and the enzymatic apparatus necessary for oxidative phosphorylation. To reach this membrane the peptides have to cross the outer bacterial membrane, consisting of lipopolysacharides (LPS) and the peptidoglycan layer, both of which are negatively charged, in a so-called "self-promoting uptake" process (*81*−*84*). The results of the diffusion potential experiment revealed that linear-K_4L_7W is up to 10-fold less active than cyclic-K_4L_7W in permeating negatively charged membranes (Figure 4A). This indicates that the existence of peptides as monomers in the membrane is very important for efficient lytic activity. Indeed, most linear α-helical antimicrobial peptides are monomeric in their membrane-bound state (*41*, *54*−*56*, *85*). Therefore, binding of linear-K_4L_7W as oligomers versus monomers of cyclic-K_4L_7W on the outer surface of the bacterial membrane makes it more difficult for the oligomer to permeate and diffuse into the inner membrane compared with the cyclic monomers. Since Gram-positive bacteria contain only one membrane, such differences are less significant.

Cyclization of linear antimicrobial peptides may have several advantages with regard to selectivity and stability, for example, the following: (i) Unfolded peptides may form aggregates because of hydrophobic interactions, leading to nonspecific adsorption to normal mammalian cells and low solubility. Placing constraints on their unfolded conformations and thus restricting exposure of hydrophobic stretches of amino acids can limit the hydrophobic interactions. Furthermore, these constraints can enhance the role of electrostatic interactions in initial binding with the negatively charged target membrane, thus substantially increasing selectivity toward bacteria versus mammalian cells. (ii) To be bound and cleaved by protease, a peptide must present the cleavage site in an extended structure. Thus, cyclization of short peptides may limit their accessibility to protease activity due to their rigid and constrained structure. (iii) Since cyclization seems to affect activity only toward Gram-negative bacteria, further studies along this line may assist in the design of bacteria-specific lytic peptides.

In summary, our results indicate that peptide linearity of an amphipathic α-helical peptide is not crucial for antibacterial activity but instead affects selectivity between Gram-positive and Gram-negative bacteria and between mammalian cells and bacteria. Since the peptides have the same sequence of hydrophobic and positively charged amino acids, their distinct binding and permeating properties can only be explained by their different propensities to oligomerize in solution and in membranes and to form a helical structure. Similar to the incorporation of D-amino acids, cyclization should destabilize the helical structure. Thus, to form a helical structure, the cyclic and the diastereomer peptides probably have to cross an energy barrier. Electrostatic interactions between the positively charged cyclic and diastereomeric peptides and the negatively charged membranes seem to allow the peptides to cross the energy barrier and form a stable helical structure required for membrane binding and lysis. Furthermore, the combination of incorporating D-amino acids into lytic peptides and their cyclization open the way for developing a new group of antimicrobial peptides for treating of infectious diseases, whose properties would be improved compared to linear ones.

REFERENCES

1. Boman, H. G. (1995) *Annu. Rev. Immunol. 13*, 61−92.
2. Oren, Z., and Shai, Y. (1998) *Biopolymers 47*, 451−463.
3. Matsuzaki, K., Sugishita, K., Ishibe, N., Ueha, M., Nakata, S., Miyajima, K., and Epand, R. M. (1998) *Biochemistry 37*, 11856−11863.
4. Wieprecht, T., Beyermann, M., and Seelig, J. (1999) *Biochemistry 38*, 10377−10387.
5. Lehrer, R. I., Lichtenstein, A. K., and Ganz, T. (1993) *Annu. Rev. Immunol. 11*, 105−128.
6. Selsted, E. M., Tang, Y. Q., Morris, W. L., McGuire, P. A., Novotny, M. J., Smith, W., Henschen, A. H., and Cullor, J. S. (1993) *J. Biol. Chem. 268*, 6641−6648.
7. Hoffmann, J. A., and Hetru, C. (1992) *Immunol. Today 13*, 411−415.
8. Kokryakov, V. N., Harwig, S. S., Panyutich, E. A., Shevchenko, A. A., Aleshina, G. M., Shamova, O. V., Korneva, H. A., and Lehrer, R. I. (1993) *FEBS Lett. 327*, 231−236.
9. Nakamura, T., Furunaka, H., Miyata, T., Tokunaga, F., Muta, T., Iwanaga, S., Niwa, M., Takao, T., and Shimonishi, Y. (1988) *J. Biol. Chem. 263*, 16709−16713.
10. Andersson, M., Gunne, H., Agerberth, B., Boman, A., Bergman, T., Sillard, R., Jornvall, H., Mutt, V., Olsson, B., and Wigzell, H. (1995) *EMBO J. 14*, 1615−1625.
11. Wu, M., and Hancock, R. E. W. (1999) *J. Biol. Chem. 274*, 29−35.
12. Tamamura, H., Ikoma, R., Niwa, M., Funakoshi, S., Murakami, T., and Fujii, N. (1993) *Chem. Pharm. Bull. (Tokyo) 41*, 978−980.
13. Qu, X. D., Harwig, S. S. L., Shafer, W. M., and Lehrer, R. I. (1997) *Infect. Immun. 65*, 636−639.
14. Andersson, M., Holmgren, A., and Spyrou, G. (1996) *J. Biol. Chem. 271*, 10116−10120.
15. Segrest, J. P., De, L. H., Dohlman, J. G., Brouillette, C. G., and Anantharamaiah, G. M. (1990) *Proteins 8*, 103−117.
16. Steiner, H., Hultmark, D., Engstrom, A., Bennich, H., and Boman, H. G. (1981) *Nature 292*, 246−248.
17. Zasloff, M. (1987) *Proc. Natl. Acad. Sci. U.S.A 84*, 5449−5453.
18. Mor, A., Nguyen, V. H., Delfour, A., Migliore, S. D., and Nicolas, P. (1991) *Biochemistry 30*, 8824−8830.
19. Habermann, E., and Jentsch, J. (1967) *Hoppe Seyler's Z. Physiol. Chem. 348*, 37−50.
20. Lazarovici, P., Primor, N., and Loew, L. M. (1986) *J. Biol. Chem. 261*, 16704−16713.
21. Shai, Y., Fox, J., Caratsch, C., Shih, Y. L., Edwards, C., and Lazarovici, P. (1988) *FEBS Lett. 242*, 161−166.
22. Epand, R. M. (1993) *The Amphipathic Helix*, CRC Press, Boca Raton, FL.
23. Andreu, D., Merrifield, R. B., Steiner, H., and Boman, H. G. (1985) *Biochemistry 24*, 1683−1688.
24. Chen, H. C., Brown, J. H., Morell, J. L., and Huang, C. M. (1988) *FEBS Lett. 236*, 462−466.
25. Shai, Y., and Oren, Z. (1996) *J. Biol. Chem. 271*, 7305−7308.
26. Oren, Z., and Shai, Y. (1996) *Biochemistry 36*, 1826−1835.
27. Oren, Z., Hong, J., and Shai, Y. (1997) *J. Biol. Chem. 272*, 14643−14649.
28. Krause, E., Beyermann, M., Dathe, M., Rothemund, S., and Bienert, M. (1995) *Anal. Chem. 67*, 252−258.
29. Rothemund, S., Beyermann, M., Krause, E., Krause, G., Bienert, M., Hodges, R. S., Sykes, B. D., and Sonnichsen, F. D. (1995) *Biochemistry 34*, 12954−12962.

30. Ladokhin, A. S., and White, S. H. (1999) *J. Mol. Biol. 285*, 1363−1369.
31. Sharon, M., Oren, Z., Shai, Y., and Anglister, J. (1999) *Biochemistry, 38*, 15305−15316.
32. Merrifield, R. B., Vizioli, L. D., and Boman, H. G. (1982) *Biochemistry 21*, 5020−5031.
33. Bartlett, G. R. (1959) *J. Biol. Chem. 234*, 466−468.
34. Papahadjopoulos, D., and Miller, N. (1967) *Biochim. Biophys. Acta 135*, 624−638.
35. Rizzo, V., Stankowski, S., and Schwarz, G. (1987) *Biochemistry 26*, 2751−9.
36. Schwarz, G., Gerke, H., Rizzo, V., and Stankowski, S. (1987) *Biophys. J. 52*, 685−692.
37. Beschiaschvili, G., and Seelig, J. (1990) *Biochemistry 29*, 52−58.
38. Sims, P. J., Waggoner, A. S., Wang, C. H., and Hoffmann, J. R. (1974) *Biochemistry 13*, 3315−3330.
39. Loew, L. M., Rosenberg, I., Bridge, M., and Gitler, C. (1983) *Biochemistry 22*, 837−844.
40. Shai, Y., Bach, D., and Yanovsky, A. (1990) *J. Biol. Chem. 265*, 20202−20209.
41. Gazit, E., Miller, I. R., Biggin, P. C., Sansom, M. S. P., and Shai, Y. (1996) *J. Mol. Biol. 258*, 860−870.
42. Surewicz, W. K., Mantsch, H. H., and Chapman, D. (1993) *Biochemistry 32*, 389−394.
43. Schägger, H., and Jagow, G. V. (1987) *Anal. Biochem. 166*, 368−379.
44. Chan, T., and Shellenberg, K. (1968) *J. Biol. Chem. 243*, 6284−6289.
45. Cowgill, R. W. (1967) *Biochim. Biophys. Acta 140*, 37−38.
46. Cornut, I., Buttner, K., Dasseux, J. L., and Dufourcq, J. (1994) *FEBS Lett. 349*, 29−33.
47. Dufourcq, J., and Faucon, J. F. (1977) *Biochim. Biophys. Acta 467*, 1−11.
48. Vogel, H. (1981) *FEBS Lett. 134*, 37−42.
49. Talbot, J. C., Faucon, J. F., and Dufourcq, J. (1987) *Eur. Biophys. J. 15*, 147−157.
50. Kiyota, T., Lee, S., and Sugihara, G. (1996) *Biochemistry 35*, 13196−13204.
51. Shaw, N. (1974) *Adv. Appl. Microbiol. 17*, 63−108.
52. Verkleij, A. J., Zwaal, R. F., Roelofsen, B., Comfurius, P., Kastelijn, D., and Deenen, L. V. (1973) *Biochim. Biophys. Acta 323*, 178−193.
53. Mao, D., and Wallace, B. A. (1984) *Biochemistry 23*, 2667−2673.
54. Pouny, Y., Rapaport, D., Mor, A., Nicolas, P., and Shai, Y. (1992) *Biochemistry 31*, 12416−12423.
55. Strahilevitz, J., Mor, A., Nicolas, P., and Shai, Y. (1994) *Biochemistry 33*, 10951−10960.
56. Gazit, E., Lee, W. J., Brey, P. T., and Shai, Y. (1994) *Biochemistry 33*, 10681−10692.
57. Gazit, E., Boman, A., Boman, H. G., and Shai, Y. (1995) *Biochemistry 34*, 11479−11488.
58. Jackson, M., and Mantsch, H. H. (1995) *Crit. Rev. Biochem. Mol. Biol. 30*, 95−120.
59. Pezolet, M., Bonenfant, S., Dousscau, F., and Papineau, Y. (1992) *FEBS Lett. 299*, 247−250.
60. Mantsch, H. H., Perczel, A., Hollosi, M., and Fasman, G. D. (1993) *Biopolymers 33*, 201−207.
61. Byler, D. M., and Susi, H. (1986) *Biopolymers 25*, 469−487.
62. Miyazawa, T. (1960) *J. Mol. Spectrosc. 4*, 168−172.
63. Tatulian, S. A., Biltonen, R. L., and Tamm, L. K. (1997) *J. Mol. Biol. 268*, 809−15.
64. Dwivedi, A. M., and Krimm, S. (1984) *Biopolymers 23*, 923−943.
65. Rothschild, K. J., and Clark, N. A. (1979) *Science 204*, 311−312.
66. Lemmon, M. A., Flanagan, J. M., Hunt, J. F., Adair, B. D., Bormann, B. J., Dempsey, C. E., and Engelman, D. M. (1992) *J. Biol. Chem. 267*, 7683−7689.
67. Simmerman, H. K. B., Kobayashi, Y. M., Autry, J. M., and Jones, L. R. (1996) *J. Biol. Chem. 271*, 5941−5946.
68. Westerhoff, H. V., Zasloff, M., Rosner, J. L., Hendler, R. W., De, W. A., Vaz, G. A., Jongsma, P. M., Riethorst, A., and Juretic, D. (1995) *Eur. J. Biochem. 228*, 257−264.
69. Ghosh, J. K., Shaool, D., Guillaud, P., Ciceron, L., Mazier, D., Kustanovich, I., Shai, Y., and Mor, A. (1997) *J. Biol. Chem. 272*, 31609−31616.
70. Oren, Z., Lerman, J. C., Gudmundsson, G. H., Agerberth, B., and Shai, Y. (1999) *Biochem. J. 341*, 501−513.
71. Matsuzaki, K., Harada, M., Funakoshi, S., Fujii, N., and Miyajima, K. (1991) *Biochim. Biophys. Acta 1063*, 162−170.
72. Jacobs, R. E., and White, S. H. (1989) *Biochemistry 28*, 3421−3437.
73. Sui, S. F., Wu, H., Guo, Y., and Chen, K. S. (1994) *J. Biochem. (Tokyo) 116*, 482−487.
74. Brock, T. D. (1974) *Biology of Microorganisms*, 2nd ed., Prentice Hall Inc., Englewood Cliffs, NJ.
75. Matsuzaki, K., Harada, M., Handa, T., Funakoshi, S., Fujii, N., Yajima, H., and Miyajima, K. (1989) *Biochim. Biophys. Acta 981*, 130−134.
76. Williams, R. W., Starman, R., Taylor, K. M., Gable, K., Beeler, T., Zasloff, M., and Covell, D. (1990) *Biochemistry 29*, 4490−4496.
77. Gomes, A. V., De Waal, A., Berden, J. A., and Westerhoff, H. V. (1993) *Biochemistry 32*, 5365−5372.
78. Matsuzaki, K., Sugishita, K., Fujii, N., and Miyajima, K. (1995) *Biochemistry 34*, 3423−3429.
79. Wieprecht, T., Dathe, M., Schumann, M., Krause, E., Beyermann, M., and Bienert, M. (1996) *Biochemistry 35*, 10844−10853.
80. Latal, A., Degovics, G., Epand, R. F., Epand, R. M., and Lohner, K. (1997) *Eur. J. Biochem. 248*, 938−946.
81. Sawyer, J. G., Martin, N. L., and Hancock, R. E. (1988) *Infect. Immun. 56*, 693−698.
82. Piers, K. L., and Hancock, R. E. (1994) *Mol. Microbiol. 12*, 951−958.
83. Piers, K. L., Brown, M. H., and Hancock, R. E. (1994) *Antimicrob. Agents Chemother. 38*, 2311−2316.
84. Falla, T. J., Karunaratne, D. N., and Hancock, R. E. W. (1996) *J. Biol. Chem. 271*, 19298−19303.
85. Schumann, M., Dathe, M., Wieprecht, T., Beyermann, M., and Bienert, M. (1997) *Biochemistry 36*, 4345−51.

BI992408I